An Acad Bras Cienc (2022) 94(Suppl.1): e20210217 DOI 10.1590/0001-3765202220210217
Anais da Academia Brasileira de Ciências | *Annals of the Brazilian Academy of Sciences*
Printed ISSN 0001-3765 I Online ISSN 1678-2690
www.scielo.br/aabc | www.fb.com/aabcjournal

GEOSCIENCES

Snowmelt retrieval algorithm for the Antarctic Peninsula using SAR imageries

CLAUDIO W. MENDES JR, JORGE ARIGONY NETO, FERNANDO L. HILLEBRAND, MARCOS W.D. DE FREITAS, JULIANA COSTI & JEFFERSON C. SIMÕES

Abstract: The classification of Synthetic Aperture Radar (SAR) images by knowledge-based algorithms with elevation and backscatter thresholds were used in several studies to detect the Wet Snow Radar Zone (WSZ) in the Antarctic Peninsula. To identify it more accurately based on its seasonal variations, this study proposed the additional use of a threshold in synthetic images, created by rationing summer and winter sigma linear images. In our algorithm we used the following thresholds to detect the WSZ in Envisat ASAR imageries, using the Radarsat Antarctic Map Digital Elevation Model as ancillary data: i) -25 dB < s^0 < -14 dB; ii) s_{linear} summer / s_{linear} winter < 0.4; iii) elevation H < 1,200 m for northern tip and H < 800 m for southern tip of the Antarctic Peninsula. The classified images were post-processed by a focal majority 5 x 5 filter and superimposed by an image of rock outcrops derived from the Antarctic Digital Database. The ratio image threshold allowed discriminating the WSZ from the Dry Snow Radar Zone and radar shadows, as well as transitional areas between this glacier zone and the Frozen Percolation Radar Zone, which would be classified incorrectly if we used only elevation and backscatter thresholds.

Key words: Antarctic Peninsula, Envisat ASAR, SAR imagery, snowmelt, Wet Snow Zone.

INTRODUCTION

The analysis of spatiotemporal variations of glacier facies, such as the Dry Snow Zone, Frozen Percolation Zone, Wet Snow Zone (WSZ), and Ablation Zone (Paterson 1994), can provide evidence of climate and glaciological changes in the Antarctic Peninsula (Rau et al. 2001, Cook & Vaughan 2010, Bevan et al. 2020). The WSZ extension, defined as the surface area of a glacier where the snowpack is saturated with water (Paterson 1994), can be used as input data in runoff modeling, to predict its impacts on local coastal environments and their contribution to sea-level rise. These glacier facies can be detected in radar imageries and when it is used this type of data they are called Radar Glacier Zones (RGZ): Dry Snow Radar Zone (DSRZ), Frozen Percolation Radar Zone (FPRZ), Wet Snow Radar Zone (WSRZ), and Bare Ice Radar Zone (BIRZ).

RGZ can be detected automatically in radar images from pixel-based or object-based classifiers. Using a Geographic Object-Based Image Analysis (GEOBIA) approach, Liu et al. (2006) delineated snow zones in a high-resolution Radarsat SAR image mosaic by segmenting it with a region growing and merging algorithm and classified RGZ based on backscatter and texture properties of these segments. Besides that, applied context classifiers for RGZ post-classification, to enable the generation of more continuous and coherent classes, according to the areal size and adjacency relationship between these glacier zones.

Zhou & Zheng (2017) and Zhou et al. (in press) mapped radar glacier zones in the Antarctic Peninsula by using Sentinel-1 images, based on backscatter coefficient and elevation thresholds, and a decision-tree classification method. Fu et al. (2020) proposed the application of a supervised Support Vector Machine (SVM) classification and a simple decision-tree classification method to detect radar glacier zones in the Antarctic Peninsula using Polarimetric SAR. They found that the polarimetric decomposition produced better glacier zones recognition because of its ability to detect scattering procedures and scattering mechanisms.

Besides GEOBIA and SVM, one of the most used techniques for RGZ classification is based on slicing SAR (Synthetic Aperture Radar) images with backscatter thresholds, as seen in Jezek et al. (1993), Partington (1998), Braun et al. (2000), Rau et al. (2001, 2004), Rau & Braun (2002), Rau (2003), Ramage & Isacks (2003), Arigony-Neto (2006, 2009), Arigony-Neto et al. (2006, 2007, 2009), Mendes Jr. et al. (2009) and Huang et al. (2013).

Arigony-Neto (2006) developed a decision rule algorithm to detect RGZ in ERS 1 and 2 AMI SAR (European Remote Sensing Satellite - Active Microwave Instrument SAR) and Envisat ASAR (Environmental Satellite - Advanced SAR). In this classification algorithm, pixels were allocated to a given RGZ in SAR images according to normalized backscatter coefficient (sigma naught - s^0) and elevation thresholds, automatically extracted from a Digital Elevation Model (DEM). In the Ph.D. thesis and derived papers published by this author (e.g., Arigony-Neto et al. 2006, 2007, 2009) the RGZ classification was performed only in glacier centerlines of the Antarctica Peninsula, to avoid geometric distortions and the topographic effects of snow and ice backscattering, which is inherent to SAR images.

Image rationing techniques can also be applied for the WSRZ classification. This methodology consists of using SAR images acquired in seasons marked by surface melting and refreezing processes in glaciers and consequently variations in radar backscatter. Based on this approach, Arigony-Neto (2009) developed a decision rule algorithm for WSRZ detection in the Antarctic Peninsula, by using s^0 thresholds defined by Rau et al. (2001) and empirical threshold values of synthetic images, derived from rationing austral summer and winter ASAR images in sigma linear scale (i.e., intensity values).

This study aims to improve these WSRZ classification methods by combining decision rules proposed by Arigony-Neto (2006, 2009) in one snowmelt retrieval algorithm, to detect this glacier facie more accurately in the Antarctic Peninsula.

GLACIER FACIES DETECTION IN RADAR IMAGES

A glacier can be defined as a mass of snow and ice that moves continuously by creep (internal deformation) or basal sliding, from a higher to a lower area. However, a glacier is not a homogeneous mass of snow and ice. It can be divided into facies or zones, according to changes of its superficial and internal characteristics (Paterson 1994), distributed in the following order, from the highest areas to its frontal position (Figure 1): Dry Snow Zone, Frozen Percolation Zone, Wet Snow Zone, Superimposed Ice zone, and Ablation Area.

The Dry Snow Zone is characterized by small grain sizes and is located in higher areas of glaciers, where there is no melting even in the summer, being restricted to areas in the interior of Antarctica and Greenland, where the

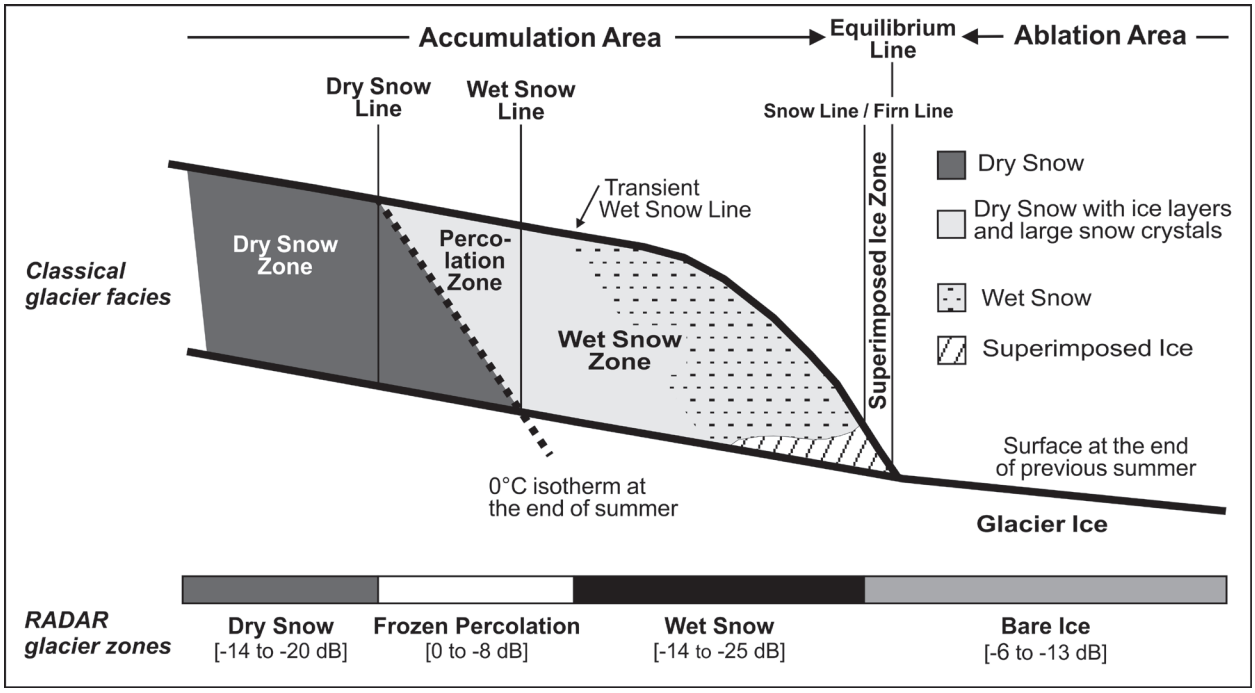

Figure 1. Classical glacier facies as described by Paterson (1994) and corresponding RADAR glacier zones as detected by SAR sensor. Modified after Rau et al. (2001).

surface air temperature never rises above the melting point. On the other hand, some surface melting happens in the Frozen Percolation Zone, and the water percolates down a few meters and refreeze, forming vertical structures (e.g., canals and ice glands) and horizontal structures (e.g., ice layers or lenses). This glacier zone is marked by large grain sizes, resulting from melt-freeze metamorphism. The Wet Snow Zone is characterized by snow with liquid water, caused by surface melting in the ablation season. The Superimposed Ice Zone presents melting water, merged ice structures like ice layers, lenses and glands, forming a continuous mass of superimposed ice. The Ablation Area is an irregular surface of exposed glacier ice, with the presence of some remaining snow and/or firn patches. Figure 1 describes the s^0 values of the RGZ for SAR images acquired in the C-band, at VV polarization, during the austral summer in the Antarctic Peninsula, according to Rau et al. (2001).

In different snow zones, the size and density of the snow grain, the stratigraphy, the surface roughness and the water content of the snowpack are different. These factors affect the surface and backscatter intensity of the radar signal volume, and hence the brightness variation in radar images. In the DSRZ, thaw does not occur even during the summer, containing a low density of snow at the top, uniform crystals of small grain size and a layer of moderate snow, with no layers of ice related to the melt. The interaction between the radar signal and the snowpack is dominated by the dispersion of the volume below the snow surface. Due to the high penetration depth (about 20 m) and predominant volume spread, the dry snow zone is characterized by low backscatter (Fahnestock et al. 1993, Jezek et al. 1993, 1994).

This low backscatter is also found for the WSRZ region, where surface melting is intense and vigorous. The top snow layer gets wet during the summer. There is a strong seasonal

dependence on the radar backscatter associated with the occurrence of the melt. During summers, the radar signal penetration depth is drastically reduced to the upper 3–4 cm due to the presence of high liquid water content in the snow cover. Increasing wet snow absorption strongly decreases the strength of backscatter intensity (Jezek et al. 1993, 1994, Partington 1998).

The different gray tones of the DSRZ and FPRZ in radar images allow identifying the percolation line, while variations in gray tones between the FPRZ (light gray) and WSRZ (dark gray) can be used to delimit the wet snow line. Besides, the position of the snow line of a glacier, which indicates the current extent of the ablation area, can be identified in the transition of the gray tones of the FPRZ and BIRZ. The vertical and horizontal structures in the FPRZ reach dimensions similar to the wavelength of the SAR, producing strong signal returns, and consequently, this RGZ has lighter gray tones in these images than the other glacier facies (Figure 1). The variations in the extent and elevation of these boundaries between glacier facies are responses to changes in energy and mass balance and, therefore, may reveal changes in local and regional glaciological and climatological conditions (Vogt & Braun 2004).

The radar data enables the spatial detection of RGZ, with the potential to reveal considerable qualitative information on the melting dynamics in the snowpack (Vogt & Braun 2004). Besides, the most suitable images for the WSRZ classification can be obtained from these active sensors even in low sunlight and under cloud cover, which are frequent conditions in the Antarctic Peninsula and which make it difficult to obtain regular images by optical sensors in this area (Bremer et al. 2004). Furthermore, optical imageries are not suitable to identify the Frozen Percolation Zone and the Dry Snow Line (DSL), because the optical properties of ice crystals radiance measured on glaciers at visible and infrared wavelengths depends on properties of a few centimeters (10-20 cm) of the snowpack, not being sensitive to the presence or absence of slight wetting or refreezing in the snowpack.

Among data from microwave active sensors, images from the ASAR sensor can be applied in the study of snow and ice masses. Onboard satellite Envisat and operating from 2002 to 2012 in the C band (i.e., 5.6 cm wavelength), the ASAR sensor can obtain images that could be used to discriminate RGZ. This sensor had a Wide Swath mode, with a spatial resolution of 150 m and 405 km swath width, therefore being applicable for studies on a regional scale, as in the case of the Antarctic Peninsula. Besides, ASAR sensor could obtain daily images of the polar regions in this acquisition mode.

THE ANTARCTIC PENINSULA

The Antarctic Peninsula is surrounded by the Bellingshausen and the Weddell seas (Figure 2). It is about 1,500 km long, extending almost longitudinally between latitudes 63° S and 75° S, being composed of an internal plateau with a mean elevation of 1,500 m. Its width varies from 35 km in the far north to almost 300 km at latitude 75° S.

In the northeast (Prince Gustav and Larsen B Ice Shelf), east and southeast (Larsen C Ice Shelf) regions of the Antarctic Peninsula, the climate is pseudocontinental, cold and dry. The climate of these regions is influenced by cold and dry winds from the Weddell Sea, and by catabatic winds from the interior of the Antarctic Ice Sheet, which is deflected by the orographic barrier of the Antarctic Peninsula plateau. The western region of the Antarctic Peninsula (George VI and Wilkins Ice Shelf) is influenced by hot and humid winds from the Bellingshausen Sea.

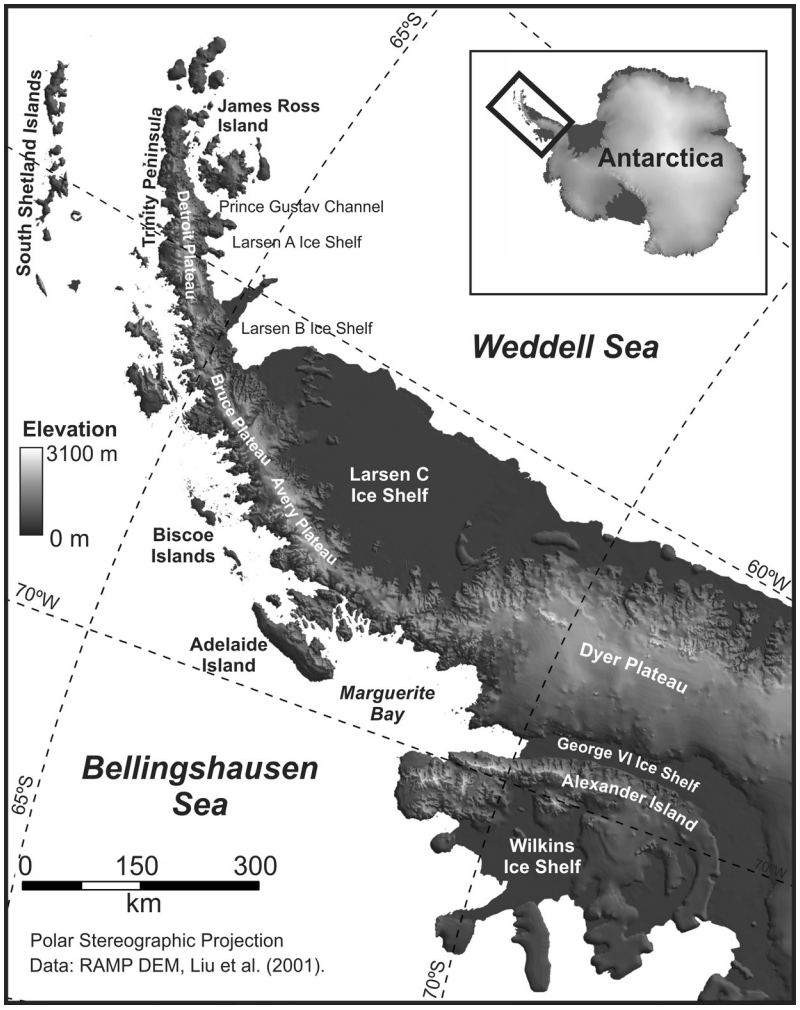

Figure 2. Location map of the Antarctic Peninsula. The Digital Elevation Model is from the Radarsat Antarctic Mapping Project (Liu et al. 2001).

The climate is maritime polar, hotter and wetter (higher precipitation rate) than the east coast of the Antarctic Peninsula. The mean annual atmospheric temperatures over the Weddell Sea is about 7°C lower than that of Bellingshausen, at points of the same latitude and altitude (Morris & Vaughan 2003).

This peninsula had strong and statistically significant warming over the last 60 years (Jones et al. 2019). Among other consequences, this warming trend caused significant changes in glacial systems of the Antarctic Peninsula, such as the reduction of seasonal sea ice, increasing trend in melting conditions, retreat of glacier fronts, and break-up and disintegration of ice shelves (Scambos et al. 2000, Cook & Vaughan 2010, Trusel et al. 2012, Bevan et al. 2020). The persistent and intense meltwater fluxes contributed to accelerate the retreat of Antarctic Peninsula ice shelves, as reported by Scambos et al. (2000), Van den Broeke (2005), Trusel et al. (2013) and Bevan et al. (2020).

MATERIALS AND METHODS

The procedures applied in this study can be divided into two main steps: image pre-processing (comprising radiometric calibration, speckle noise filtering, and geometric data corrections) and the WSRZ detection in ASAR images, covering the Antarctic Peninsula.

Pre-processing of ASAR images

To cover the entire continental area of the Antarctic Peninsula, we used three ASAR images on the wide swath mode at VV polarization. To analyze melting and re-freezing events of the snow, we used ASAR images of November 2006, of the ablation periods in Antarctica (i.e., between December and February) of 2006/2007, and of March and April 2007. Besides, ASAR images from the austral spring and winter of 2006 and austral autumn of 2007 were used for their application in our WSRZ classification method. The complete list of ASAR WS images used in this study is described in Table I.

The ASAR WS images used in this study were type 1P, a multi-look detected product with radiometric corrections related to the antenna, without georeferencing and corrections for the radiometric effects induced by the illuminated terrain, with data in the ground range projection (ESA 2007). These images were imported into the Sentinel Application Platform (SNAP), which is a free software developed by the European Space Agency (ESA 2020) for processing images from

Table I. Date of acquisition and track/frame of ASAR images on wide swath mode (VV polarized) used in the classification of the Wet Snow Zone in the Antarctic Peninsula.

ASAR classified images (dB and linear scales)				ASAR reference images (linear scale)			
Date	**Track**	**Frame**	**Polar.**	**Date**	**Track**	**Frame**	**Polar.**
11/15/2006	23*	1149, 1155	VV	06/28/2006	23*	3259, 3321	VV
		1153		08/02/2006		3265	
11/21/2006	109	1163, 1167	VV	07/04/2006	109	3263, 3187	VV
		1165		09/12/2006		3253	
12/01/2006	252*	1169, 1173	VV	06/28/2006	23*	3259, 3321	VV
		1171		08/02/2006		3265	
12/07/2006	338	1175, 1179	VV	07/20/2006	338	3277, 3275	VV
		1177		06/15/2006		3179	
12/20/2006	23*	1181, 1185	VV	06/28/2006	23*	3259, 3321	VV
		1183		08/02/2006		3265	
12/23/2006	66	1187, 1189, 1040	VV	06/16/2007	66	3267, 3269, 3323	VV
12/26/2006	109	1042, 1046	VV	07/04/2006	109	3263, 3187	VV
		1143		09/12/2006		3253	
01/05/2007	252*	1048, 1052	VV	06/28/2006	23*	3259, 3321	VV
		1050		08/02/2006		3265	
01/24/2007	23	1054, 1058	VV	06/28/2006	23*	3259, 3321	VV
		1056		08/02/2006		3265	
01/27/2007	66	1060, 1145, 1123	VV	06/16/2007	66	3267, 3269, 3323	VV
02/12/2007	295*	3715, 3719	VV	06/28/2006	23*	3259, 3321	VV
		3717		08/02/2006		3265	
03/03/2007	66	3307, 3305, 3303	VV	06/16/2007	66	3267, 3269, 3323	VV
03/22/2007	338	3295, 3291	VV	07/20/2006	338	3277, 3275	VV
		3293		06/15/2006		3179	
04/10/2007	109	3285, 3281	VV	07/04/2006	109	3263, 3187	VV
		3283		09/12/2006		3253	

*** Images from the tracks # 23, 252 and 295 were acquired with the same antenna incidence angle.**

several SAR sensors, including Envisat ASAR. The SNAP toolboxes were used for the radiometric calibration, speckle filtering, georeferencing and orthorectification of these images, performed by a processing workflow built in that software.

The radiometric calibration of ASAR images in SNAP was based on Rosich & Meadows (2004), where the main input parameters are the incidence angle, the absolute calibration constant, the antenna gain pattern and the range spread loss (ESA 2007).

The speckle noise filtering was the next step in our processing workflow. We applied a median 3x3 filter, which effectively reduced the speckle, while at the same time preserved edges between the glacier zones. Besides, median filter, in addition to being a simple and easy computational method, requires a relatively low processing time compared to other filters (Rees & Satchell 1997) and could be considered as one of the most efficient methods used in SAR image filtering for the RGZ classification (Arigony-Neto 2006).

In orthorectification, SNAP uses embedded metadata of SAR images (i.e., acquisition geometry, sensor parameters, orbit and ephemeris data) and elevation data from an external DEM. For that, we used the Radarsat Antarctic Mapping Project - RAMP (Liu et al. 1999, 2001), which has a spatial resolution of 200 m and coordinates in the polar stereographic projection system, which was converted to geographical coordinates, and referenced to the World Geodetic System 1984 (WGS84). These are the same cartographic references of ASAR metadata and were also used to generate the orthorectified ASAR images, resampled by the nearest neighbor interpolation method, which better preserves the original backscatter values than bilinear or cubic convolution methods.

The orthorectified images were exported to GeoTiff format and imported into ERDAS Imagine™ (Leica geosystems, Inc.), which was used for the conversion of geographical coordinates to the Lambert azimuthal equal-area projection system, which is recommended by the Scientific Committee on Antarctic Research (SCAR) for the quantification of areas and distances in polar regions, on maps of scales greater than 1:1,000,000 (SCAR 2000).

Wet Snow Radar Zone classification in ASAR images

The orthorectified ASAR WS images were used in the WSRZ classification of glaciers in the Antarctic Peninsula. The vector file of the ADD coastlines (Gerrish et al. 2020a) was used to mask ASAR data located only in the continental area of the Antarctic Peninsula. Subsequently, we performed the WSRZ classification in ASAR WS mosaics, applying the classification algorithm by decision rules developed by Arigony-Neto (2006, 2009), implemented in the Spatial Modeling Language (SML) of Erdas Imagine™ software. In the algorithm proposed by Arigony-Neto (2006), the WSRZ was classified according to backscatter thresholds (-14 dB > s^0 > -25 dB), based on Rau et al. (2001), and to elevation (H) thresholds of the northern and southern tips of the Antarctic Peninsula (H < 1200 m for the northern tip and H < 800 m for the southern one), defined by Rau & Braun (2002) and Rau (2003).

The northern and southern boundaries of the Antarctic Peninsula were digitized as polygons and were after converted to the raster format. Each of these regions was assigned with a distinct attribute and its values were used in the classification algorithm. The elevation thresholds make it possible to discriminate the DSRZ from the WSRZ, because they could have the same radar backscatter values, between -14 dB and -20 dB (Rau et al. 2001).

In our snowmelt retrieval algorithm, we used simultaneously the thresholds defined

by Arigony-Neto (2006, 2009) for the WSRZ classification. In addition to the backscatter thresholds of Arigony-Neto (2006), based on Raul et al. (2001) (Figure 1), the classification algorithm of Arigony-Neto (2009) has a threshold for synthetic images calculated from rationing ASAR images in sigma linear scale acquired from the ablation and accumulation periods, respectively. This author observed that pixels with values less than 0.4 in synthetic images resulting from rationing SAR images of summer (or obtained close to this season) and winter, both on the linear sigma scale ($s_{linear\ summer}$ / $s_{linear\ winter}$ < 0.4), correspond to WSRZ areas. This condition is also met when a given co-registered pixel of ASAR images has a backscatter value between -14 dB and -25 dB.

After the WSRZ detection, we applied a focal majority 3 x 3 filter in the WSRZ classified images, for clumping isolated and misclassified pixels, to generate more contiguous and coherent classes, following the classification algorithm proposed by Arigony-Neto (2009). This filter allows, starting from a pre-established window size, to replace cells of a raster based on the value found in most of its contiguous neighbor cells. For this to occur, two criteria must be previously met. The first is that the number of neighboring cells of a similar value must be large enough (being most or half of all cells) and these cells must be contiguous around the center of the filter core. The second criterion is related to the spatial connectivity of cells, minimizing the corruption of cellular spatial patterns (ESRI 2021).

Our classification algorithm was not developed for the rock outcrops detection, due to the similarity of their radar backscatter with the FPRZ and BIRZ. Thus, the WSRZ classified images were overlapped with the rock outcrops delimitation of the Antarctic Digital Database (ADD) (Gerrish et al. 2020b). The remaining continental areas of the Antarctic Peninsula were called a Dry Snow and Ice Radar Zone (DSIRZ), characterized by the absence of snow with liquid water, comprising the DSRZ, FPRZ and BIRZ. The processing workflow used in the WSRZ classification in ASAR WS images (Figure 4) is presented in Figure 3.

To improve the classification of glacier zones, we mapped the mean air temperature at 2 meters (T2m) of the period between the date range of the Envisat ASAR images, allowing us to visualize the relationship of the evolution of the WSZ area with the T2m. Furthermore, the regions with DSRZ can be identified based on the DSL delimitation in which there is an air temperature isotherm of -11° C (Peel 1992), represented together in the maps. Researchers such as Storvold & Malnes (2004) and Zhou et al. (in press) used air temperature data to improve the ranking between the DSRZ and WSRZ.

T2m data were obtained using the atmospheric reanalysis model European Reanalysis Agency 5 (ERA5), made available by the European Center for Medium-Range Weather Forecasts (ECMWF). The data used have a spatial resolution of 0.25° x 0.25° and daily temporal resolution. Tetzner et al. (2019) and Hillebrand et al. (2021) indicate the use of ERA5 in relation to its predecessor ERA-Interim, as it presents a better accuracy of T2m in regions with high altitudes.

RESULTS AND DISCUSSION

The decision rules of our snowmelt retrieval algorithm associate a given pixel of one ASAR WS mosaic to a WSRZ when all threshold values are met in this SAR image (radar backscatter), RAMP DEM (elevation data) and the correspondent ASAR synthetic image (ratio value). The results of the application of these decision rules for all

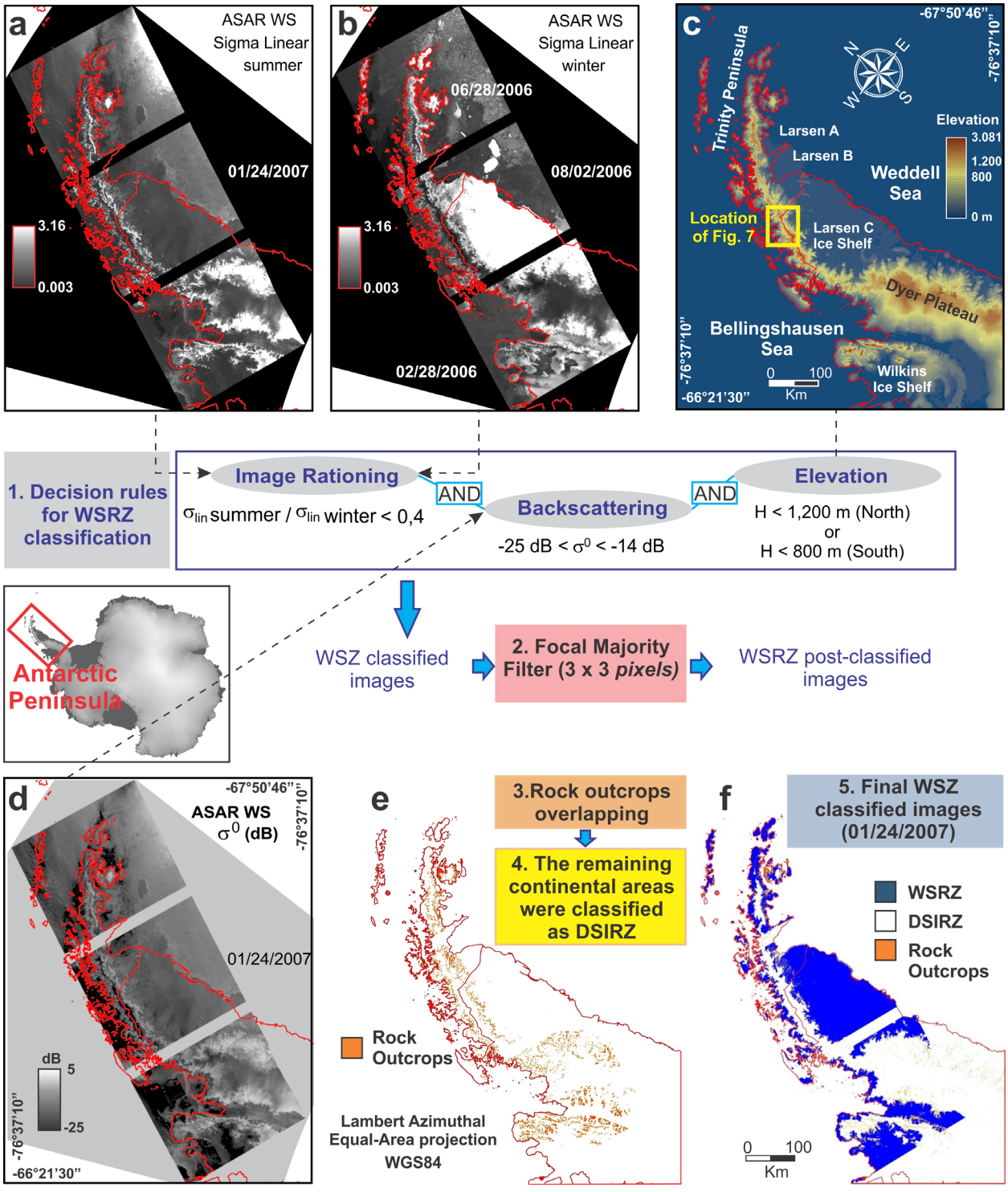

Figure 3. Snowmelt retrieval algorithm for the Antarctic Peninsula using ASAR images. In this example, we describe the classification of images acquired on January 24th, 2007. The Wet Snow Radar Zone (WSRZ) classified image was post-processed by a focal majority filter with 5 x 5 pixels and then overlapped by a rock outcrops image derived from the Antarctic Digital Database. The unclassified continental areas were assigned to Dry Snow and Ice RADAR Zones (DSIRZ), which comprises the Dry Snow Radar Zone, Frozen Percolation Radar Zone and Bare Ice Radar Zone. The location of image subsets from Figure 7 is indicated by a yellow rectangle.

Envisat ASAR images classified in this study area are presented in Figure 4.

The RGZ does not correspond to the classical glacier facies as described by Paterson (1994). The backscattering values measured on glaciers depend on sensor characteristics (e.g., wavelength, incidence angle, polarisation) and snowpack parameters (e.g., liquid water content, snow density, stratigraphy, grain size, and surface roughness). Thus, RGZ is determined by the superficial properties of glaciers, while the classical glacier facies depend on the properties of the entire snowpack from the last accumulation season (Paterson, 1994).

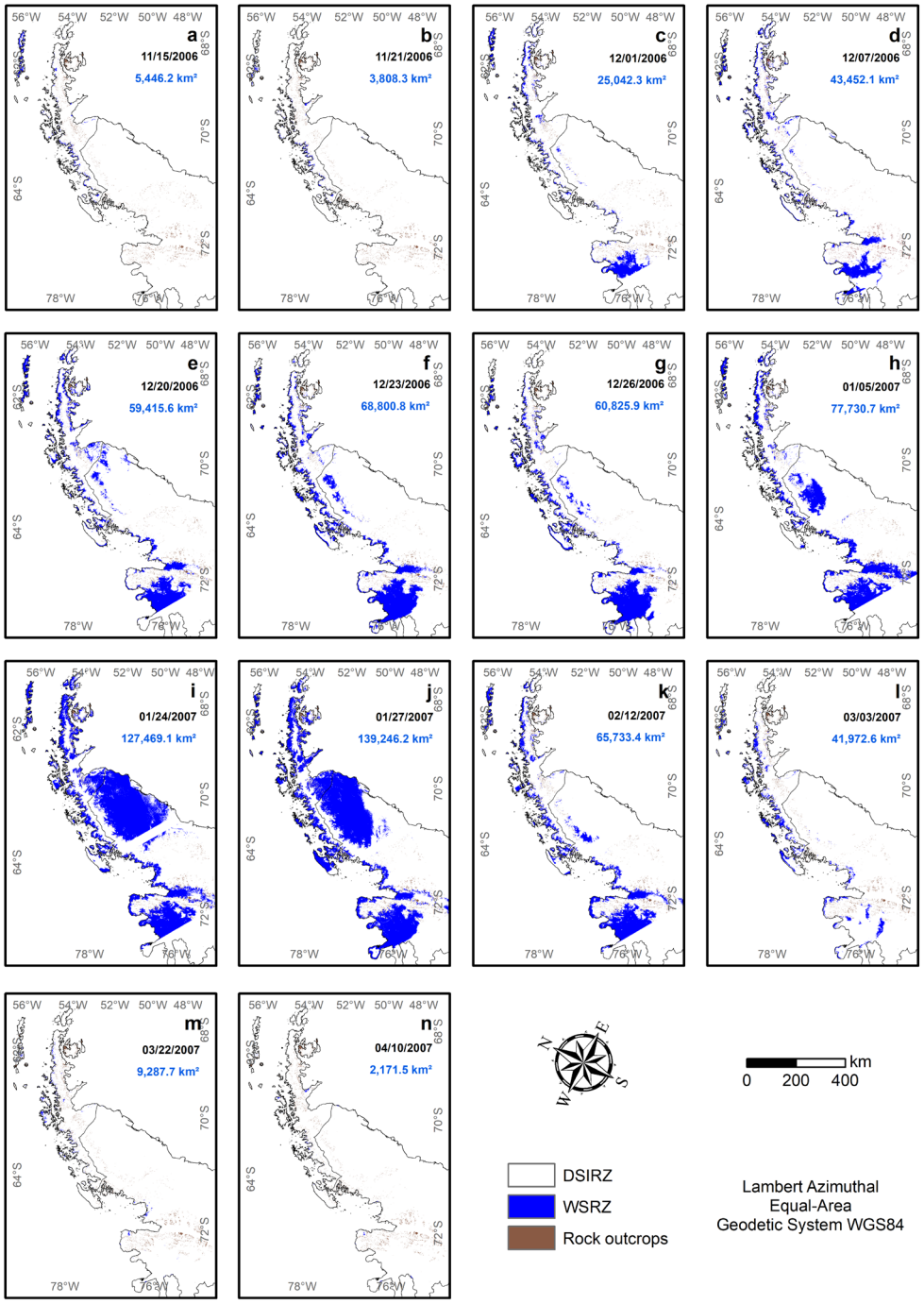

Figure 4. Classified ASAR images of the Antarctic Peninsula (Wet Snow Radar Zone – WSRZ; Dry Snow and Ice Radar Zones – DSIRZ; and rock outcrops), with their respective dates of acquisition and quantified superficial snowmelt areas (km2).

Nevertheless, the position of the limits between RGZ (i.e., DSL, wet snow line, snow line, and glacier frontal position) is considered a proxy for glacier mass balance and recent meteorological conditions (Arigony-Neto 2006).

The RGZ backscatter values vary seasonally. Throughout the year, the FPRZ has the greatest radar backscatter, appearing in lighter gray tones in SAR images. In this glacier zone, the successive events of melt-freeze metamorphism generate large snow grains, which causes strong volume backscattering. In the summer, higher backscatter values occur in the BIRZ (medium gray tones in the images), while lower values (darker gray tones) in the DSRZ and WSRZ (Figure 1).

Snow melting occurs during the ablation period in the WSRZ areas and, consequently, radar backscatter decreases due to the microwave absorption by the liquid water content, while in winter, backscatter increases due to the refreeze of the liquid water. According to Liu et al. (2006), the surface melting areas in the Antarctic continent generally expand from the coast toward the interior, from lower to higher latitude (latitudinal factor), and from lower to higher elevation (elevation factor). The longitudinal factor is also very important for the Antarctic Peninsula, because the eastern and western regions have different climate types.

To relate the climatic factor with the evolution of the WSRZ area, Figure 5 shows the maps of T2m averages between the image dates, obtained through the atmospheric reanalysis model ERA5 for the continental and oceanic regions located near the Antarctic Peninsula. By relating Figure 4 to Figure 5, we observe that the enlargement of the WSRZ area is linked with the retraction to the south of the -11°C isotherm, the threshold temperature for mapping the DSRZ regions (Peel 1992). Zhou et al. (in press) also used this type of delimitation between DSRZ and WSRZ in intense melting events with analogous backscatter characteristics.

In our time series analysis of ASAR images (Nov. 2016 – Mar. 2017), we observed that the snowmelt onset was in mid-November 2006 (Figures 4a and 4b), in the northwest region of the Antarctic Peninsula. This region is characterized by the highest surface air temperatures, and the greatest seasonal and interannual variability of the Antarctic Peninsula (Skvarca & De Angelis 2003). Snowmelt areas were detected on the South Shetland Islands, where a mean surface air temperature of about -2.30 ±0.5 °C on 11/15/2006 was recorded by the ERA5 model (Figure 5a). We also detected some snowmelt on glaciers in the northwest (Trinity Peninsula) and west regions of the Antarctic Peninsula (until latitude 67° S – near Adelaide Island), except on the Detroit, Bruce and Avery plateaus.

In early December 2006 (Figure 4c), the northwestern surface melt areas increased, finally appearing in the northeastern region of the Antarctic Peninsula. In addition, surface melt was detected in the Wilkins and George VI ice shelves (SW of the Antarctic Peninsula), in remnants of the Larsen B ice shelf (NE), and the northern region of the Larsen C ice shelf (E). In the lower elevation areas, located in the Larsen C ice shelf, were observed greater variations in backscattering, varying from lighter gray tones (0 to -8 dB) to darker ones (-14 to -20 dB). The former corresponds to a FPRZ, with strong backscatter from subsurface ice layers, and the latter to a WSRZ, because the major liquid water content in the snowpack in these areas absorbed drastically the radar signal, as detected in ASAR images from January 2007.

From January 2007 (Figure 4h) these melt areas expanded to the southern region of the Larsen C ice shelf, reaching their maximum extent at the end of that month (Figure 4j). In early February 2007 (Figure 4k), the melt areas

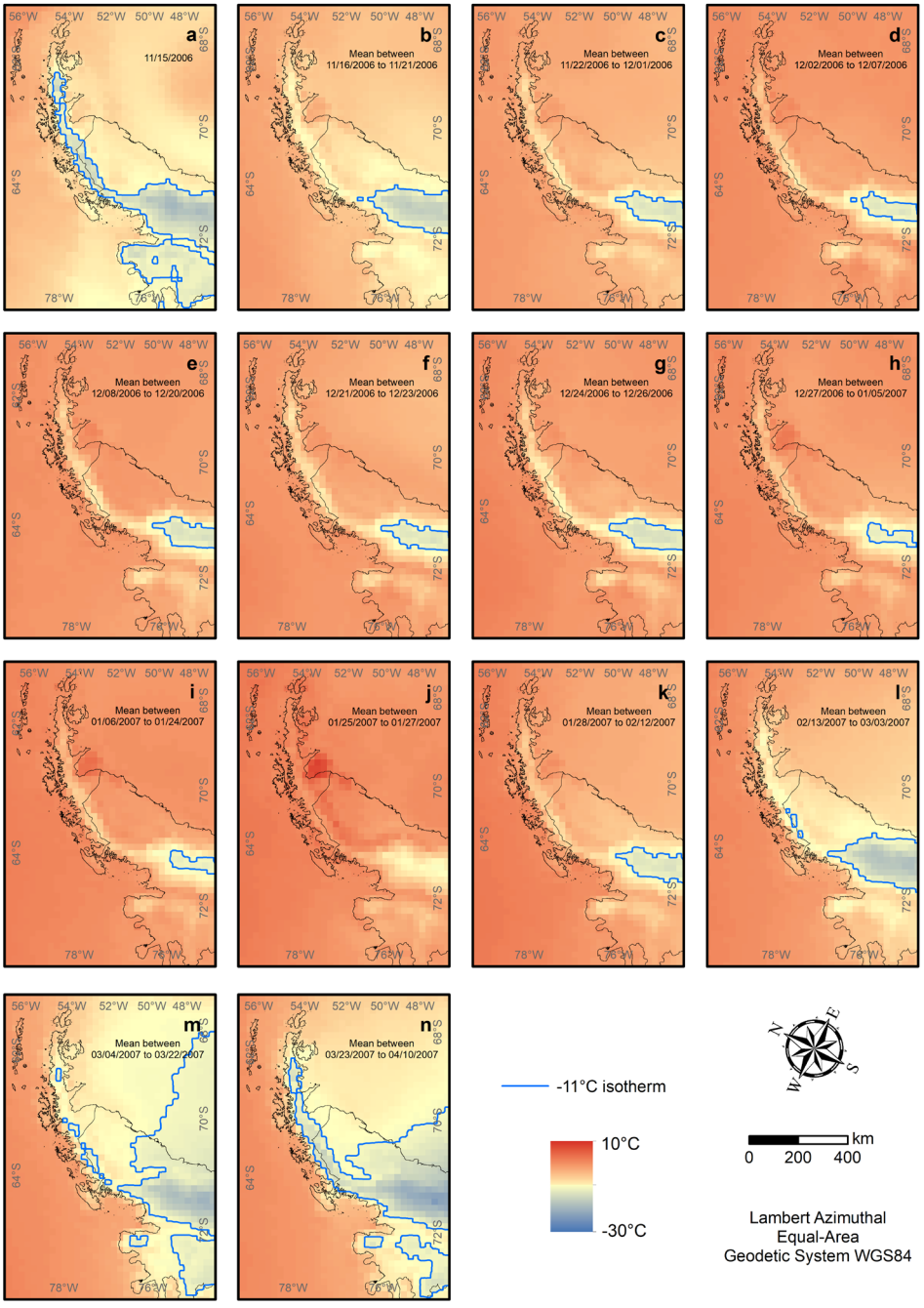

Figure 5. Spatialization of T2m in the oceanic and continental regions of the Antarctic Peninsula, obtained of the atmospheric reanalysis model ERA5, for the period covered by the radar glacier zone mapping.

on the Larsen C platform began to significantly reduce, when the mean surface air temperature was about 4.31 ± 1.75 °C (Figure 5k).

In subsets of ASAR WS images covering the Larsen C ice shelf and the Bruce plateau (Figure 6), acquired during the austral summer of 2006-2007, it can be observed in the highest areas of the Bruce plateau that the DSRZ had lower backscatter values (-14 to -25 dB) because there is no melting in the superficial snowpack. In the same area at the end of February, liquid water was refrozen in the snowpack, and the WSRZ turned into a FPRZ class (Figure 6d). This month the reduction in melt areas was less intense on the Wilkins and George VI ice shelves, where the surface air temperature was higher. This was

because glaciers in the western region may have higher surface air temperatures than those in the eastern region of the Antarctic Peninsula, even if they are at higher latitudes, due to influences from the maritime polar climate.

The WSRZ could be discriminated from the FPRZ and BIRZ only with backscatter thresholds of Rau et al. (2001). However, the WSRZ and DSRZ have similar backscatter values (-14 to -20 dB) and it is necessary an additional elevation threshold to discriminate them, but some issues will occur with the same backscatter ranges between these glacier zones and radar shadows. Glacier zones with greater variations of backscatter values in SAR images during the ablation and accumulation periods could be a WSRZ class since the synthetic image had a value greater than or equal to 0.4. This ratio threshold in SAR synthetic images allows to discriminate the WSRZ from radar shadows and also from the DSRZ, which have low or no backscatter seasonal variations, with ratio values close or equal to 1. Other techniques are also applied to detect very similar changes in backscattering, such as the Baghdadi algorithm and the Nagler algorithm that allow the detection of similarities. For this, the current SAR image of wet snow (σws) is compared to a reference image (σref) from a period when the snow is dry, or a period when the ground is not covered with snow, setting to

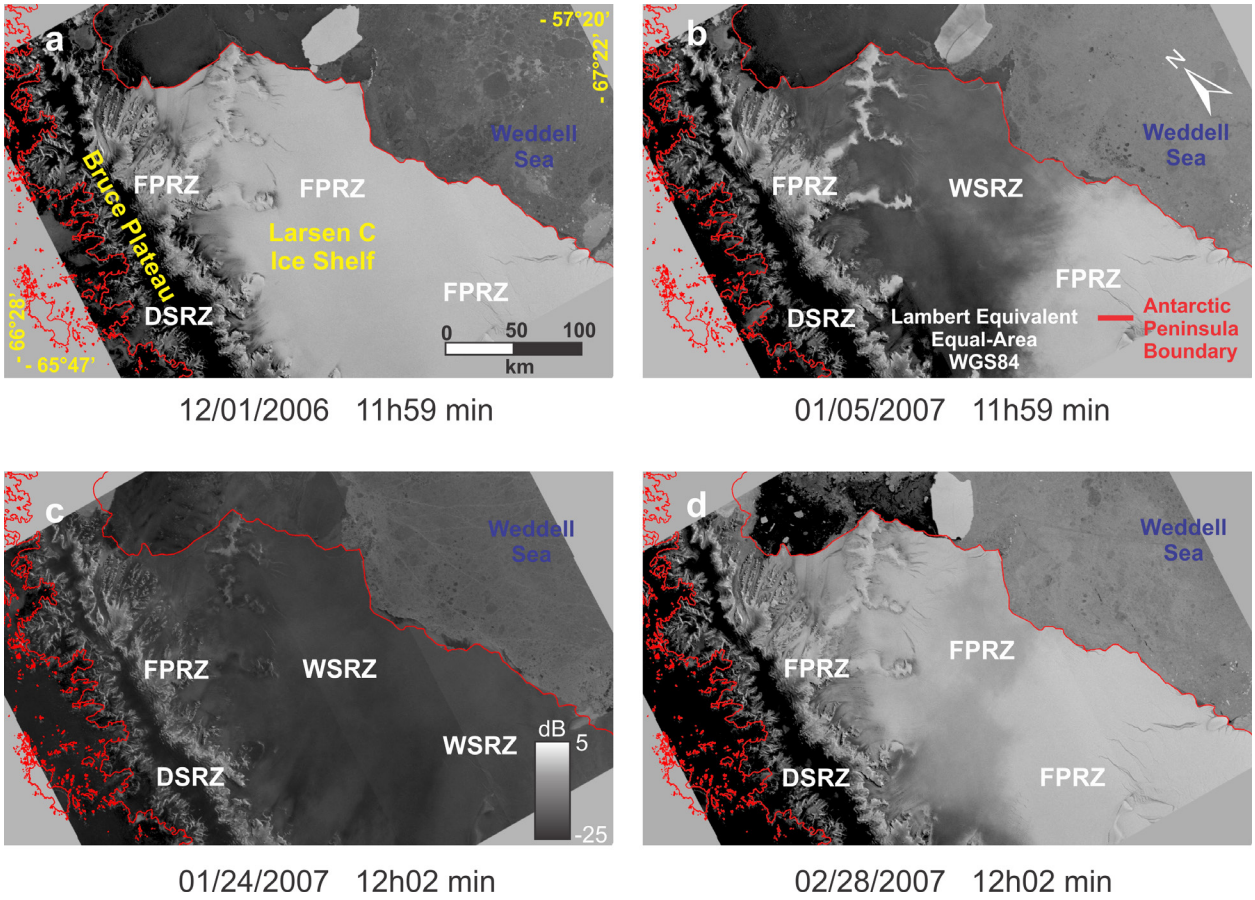

Figure 6. Subset of ASAR image on wide swath mode used in this study (dB scale), acquired in the austral summer of 2006-2007, covering the Larsen C ice shelf and the Bruce plateau. Dry Snow Radar Zone (DSRZ), Percolation Radar Zone (FPRZ) and Wet Snow Radar Zone (WSRZ) areas were classified in these images based on their backscatter values. The lighter gray tones represent higher backscatter values from the FPRZ areas, while the darker ones represent smaller backscatter values from the DSRZ and WSRZ areas.

pixels where (σws /σref) < -3 dB as wet snow (Thakur et al. 2013). As this type of relationship between images is very spatially limited, this analysis was not applied to the Antarctic Peninsula.

Figure 7 shows two subsets of ASAR WS images with backscatter values in linear scale, acquired in the austral summer (01/24/2007) and winter (02/08/2007). In the Avery Plateau, where elevation is higher than 1.200 m, darker gray tones (Figure 7c) and no seasonal variation of gray tones (Figures 7a and 7b) were observed in ASAR images, because there was no melting on the superficial snowpack, which is characteristic of the DSRZ. This elevation threshold of Arigony-Neto (2006), used in our classification algorithm, is in the agreement with Fu et al. (2000). These authors classified glacier zones in ENVISAT ASAR

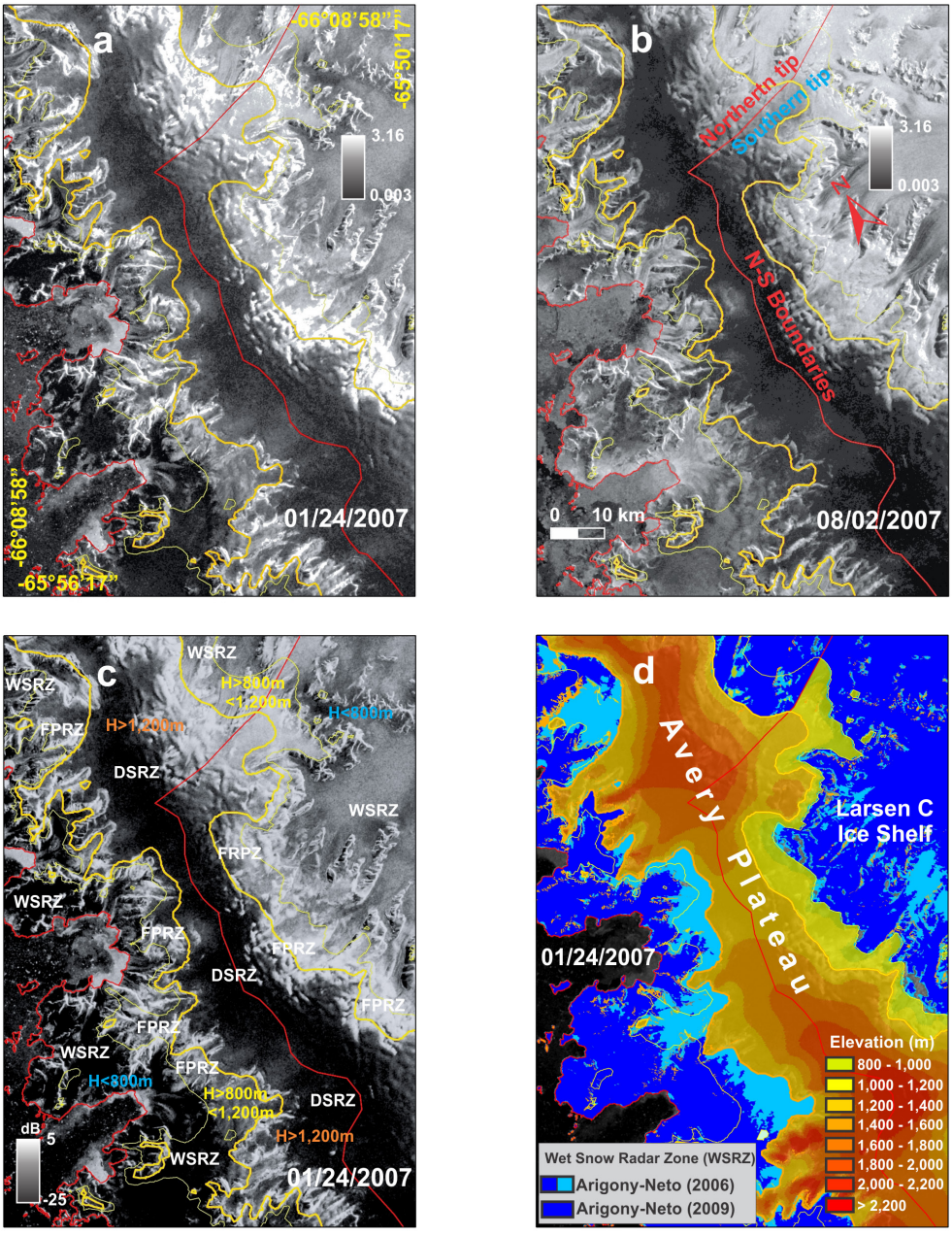

Figure 7. Subsets of ASAR images acquired on 01/24/2007, in linear (a) and decibel (c) scales, and on 02/08/2006, in linear scale (b). The location of these image subsets is shown as a yellow rectangle in Figure 3c. The elevation thresholds of 1,200 m and 800 m were used for the northern and southern tips of the Antarctic Peninsula in our snowmelt retrieval algorithm. In image C, we identified the Frozen Percolation Radar Zone (FPRZ), Wet Snow Radar Zone (WSRZ) and Dry Snow Radar Zone (DSRZ) based on elevation and backscatter thresholds. In the classified ASAR image d, we mapped the elevation data from the RAMP Digital Elevation Model, and the classified WSRZ areas resulted from the application of decision rules proposed by Arigony-Neto (2006, 2009).

wide swath images with HH polarization and full-polarimetric Radarsat-2 images, and based on ICESat (Ice, Cloud, and Land Elevation Satellite) DEM and ASTER (Advanced Spaceborne Thermal Emission and Reflection Radiometer) stereo images, found a mean elevation of about 1,200 m for the transition of DSRZ from the FPRZ on the northern Antarctic Peninsula.

Figure 7c shows the ASAR WS mosaic from 01/24/2007 with backscatter values in decibels and the identification of glacier zones with the elevation thresholds used in our snowmelt retrieval algorithm. We can observe that in areas with elevation lower than our thresholds in Figure 7c (800 m in the southern tip and 1,200 m in the northern tip of the Antarctic Peninsula) there was a variation from darker gray tones (lower backscatter - Figure 7a) to lighter gray tones (higher backscatter - Figure 7b). In Figure 7d, the WSRZ areas classified by the decision rules used in this study (i.e, based on Arigony-Neto 2006, 2009) were mapped in dark blue color, while in dark and light blue are the WSRZ areas classified by using the elevation and backscatter thresholds defined by Arigony-Neto (2006).

The evaluation of the WSRZ classification accuracy was not carried out in this study, due to the large extension of the study area, which covers the entire area of the Antarctic Peninsula. We observed the WSRZ area classified by using decision rules from Arigony-Neto (2009) will always be smaller than that of Arigony-Neto (2006), since in the former algorithm the image ratio criteria must be met in addition to the backscatter thresholds of the RGZ. In Figure 7d, the WSRZ detected by the decision rules from Arigony-Neto (2006) included all WSRZ areas detected by the Arigony-Neto (2009) algorithm, in addition to RADAR shadows and transition areas between the WSRZ and FPRZ (i.e, from -8 to -14 dB). These transitional areas within the percolation and wet snow zones seen in the multi-temporal SAR imagery could be explained by the presence of some snowmelt in the FPRZ, which in summer lowers the s^0 by a large amount, as reported by Partington (1998), Mora et al. (2013) and Fu et al. (2020). They would not be classified as WSRZ by the Arigony-Neto (2009) algorithm, which was applied in this study, as small seasonal variations of their backscatter resulted in ratio images with values greater than our defined threshold equal to 0.4.

With the application of our image rationing technique, we can identify ambiguities existing between the DSRZ and WSRZ, the FPRZ with other illuminated targets (such as rock outcrops). Furthermore, in SAR images there can be ambiguities between the backscattered signals from the FPRZ with geometric effects related to relief displacement of foreshortening and inversion of features (layover), and from the DSRZ and WSRZ with radar shadowing (Liu et al. 2006). These ambiguities cannot be detected by the pixel allocation technique and, therefore, our image rationing technique can be used as a way to discriminate RGZ from geometric effects caused by induced-relief geometric distortions, thus improving the classification process. Other ways of discriminating RGZ from these geometric relief effects would be to segment SAR images, classify segments related to these geometric effects and then apply topological neighborhood rules to assign them to a given RGZ class, as proposed by Liu et al. (2006), or following the procedures of Fu et al. (2020), that discriminated dry and wet glacier zones in full-polarimetric data by a supervised SVM classification and a decision-tree classification method.

For the correct application of our image rationing technique, the SAR images acquired in the ablation and accumulation periods must have been obtained with the same incidence angle, wavelength, amplitude, phase, polarization and acquisition mode. The

reference images should preferably be from the winter before or after the ablation images, so that the WSRZ variations represent the seasonal cycle of ablation and accumulation periods. This way, cumulative effects on the superficial glacier facies are attenuated by processes of ablation (snow melting, evaporation, calving, wind erosion, avalanches, etc.) or accumulation (precipitation of snow, ice or rain, transport of snow and ice to a glacier, avalanches, etc.).

CONCLUSIONS

Based on the results obtained in this study, it is recommended the combined use of image slicing and rationing techniques to improve the WSRZ detection accuracy in ASAR images of the Antarctic Peninsula. The former technique corresponds to a backscatter and elevation thresholds from Arigony-Neto (2006), and the latter to a threshold for synthetic images from Arigony-Neto (2009), calculated by rationing images from the accumulation and ablation periods, respectively.

The decision rules proposed by Arigony-Neto (2006) were developed for the RGZ classification in buffer zones along the glacier centerline, where the geometric effects related to relief displacement in SAR images are insignificant. The use of elevation and backscatter thresholds proposed by Arigony-Neto (2006) is recommended if this classification algorithm is performed for a glacier centerline and not for its entire catchment area. Another advantage of this algorithm is the use of only one SAR image with backscatter values, instead of using this one and two other SAR images in the sigma linear scale, as proposed by Arigony-Neto (2009) and in our snowmelt retrieval algorithm. However, for the WSRZ classification in the entire area of a glacier, we recommend the additional use of the image ratio threshold proposed in these more recent studies, which improved the classification accuracy.

Our snowmelt retrieval algorithm allowed us to discriminate the WSRZ from the DSRZ and radar shadows, which have similar backscatter because it is based on the image rationing technique developed by Arigony-Neto (2009). The additional elevation thresholds for the southern and northern tips of the Antarctic Peninsula from Arigony-Neto (2006) are also recommended in the WSRZ classification, to ensure this RGZ does not occur at elevations higher than these thresholds, where there is no melting in the snowpack.

The decision rules can only be applied for SAR images acquired in the C band, at VV polarization, and for melting areas of the Antarctic Peninsula since the RGZ backscatter thresholds of Rau et al. (2001) were defined at this wavelength and polarization. Besides ASAR images (2002-2012), the superficial snowmelt in this peninsula can be monitored by images acquired from the Active Microwave Instrument, onboard the European Remote Sensing (ER) satellites 1 (1991-2000) and 2 (1995-2011), and more recently by images from Sentinel 1A (2014 onwards) and 1B (2016 onwards) satellites, allowing to analyze spatiotemporal variations of snowmelt in long-term continuous observations.

In the context of a great debate on global climate change and the instability of Antarctic ice shelves, continuous and accurate monitoring of the WSRZ is of great importance to assess its possible impacts on glacial systems and local coastal environments, runoff modeling, and contributions to sea-level rise.

Acknowledgments

The European Space Agency (ESA) for supplying ENVISAT ASAR data within CryoSat Data Announce of Opportunity - AO (Project 2658), "Evaluating Cryosat's potential contribution to the quantification of mass balance and mass balance variations on the Antarctic Peninsula", and the ESA International Polar Year (IPY) 2007-2008 AO (Project 4032), "EO-derived products in support of climate change impact studies on the Antarctic Peninsula and Svalbard - interaction of glaciers, climate, terrestrial and marine ecosystems as well as the atmosphere".

REFERENCES

ARIGONY-NETO J. 2006. Monitoring glacier parameters on the Antarctic Peninsula – a centerline approach combining satellite and GIS data. Doctoral Thesis, Freiburg University, 136 p.

ARIGONY-NETO J. 2009. An automatic algorithm for monitoring the melting zone of the Antarctic Peninsula using ASAR WS data. In: MOCA: OUR WARMING PLANET, 9., Montreal. Proceedings ..., Montreal, p. J16.3.

ARIGONY-NETO J, RAU F, SAURER H, JANA R, SIMÕES JC & VOGT S. 2007. A time series of SAR data for monitoring changes in boundaries of glacier zones on the Antarctic Peninsula. Ann Glaciol 46: 55-60.

ARIGONY-NETO J, RAU F, SAURER H, SIMÕES JC, JAÑA R, VOGT S & GOSSMANN H. 2009. Spatial and temporal changes in dry-snow line altitude on the Antarctic Peninsula. Clim Change 94: 55-60.

ARIGONY-NETO J, SAURER H, JAÑA R, RAU F, SIMÕES JC & GObMANN H. 2006. Monitoring snow parameters on the Antarctic Peninsula using satellite data: a new methodological approach. EARSel e Proceedings 5: 100-110.

BEVAN S, LUCKMAN A, HENDON H & WANG G. 2020. The 2020 Larsen C Ice Shelf surface melt is a 40-year record high. Cryosphere 14: 3551-3564.

BRAUN M, RAU F, SAURER H & GOßMANN H. 2000. Development of radar glacier zones on the King George Island ice cap, Antarctica, during the austral summer 1996/97 as observed in ERS-2 SAR-data. Ann of Glaciol 31: 357-363.

BREMER UF, ARIGONY-NETO J & SIMÕES JC. 2004. Teledetecção de mudanças nas bacias de drenagem do gelo da ilha Rei George, Shetlands do Sul, Antártica, entre 1956 e 2000. Pesqui Antart Bras 4: 37-48.

COOK AJ & VAUGHAN DG. 2010. Overview of areal changes of the ice shelves on the Antarctic Peninsula over the past 50 years. TC 4: 77-98.

ESA. 2007. ASAR product handbook. Retrieved from <http://envisat.esa.int/ dataproducts/asar/CNTR.htm>. Accessed on Oct. 12, 2020.

ESA. 2020. Sentinel Application Platform (SNAP) user manual**.** Version 3C. Retrieved from <http://step.esa.int/main/doc/tutorials/>. Accessed on Oct. 12, 2020.

ESRI. 2021. ARCMAP. Majority Filtering. Retrieved from <https://desktop.arcgis.com/en/arcmap/latest/tools/spatial-analyst-toolbox/majority-filter.htm>. Accessed on Aug. 23, 2021.

FAHNESTOCK MA, BINDSCHADLER R, KWOK R & JEZEK KC. 1993. Greenland ice sheet surface properties and ice dynamics from ERS-1 SAR imagery. Science 262: 1530-1534.

FU W, LI X, WANG M & LIANG L. 2020. Delineation of Radar Glacier Zones in the Antarctic Peninsula Using Polarimetric SAR. Water 12: 1-16.

GERRISH L, FRETWELL P & COOPER P. 2020a. High-resolution vector polylines of the Antarctic coastline (7.3) [Data set]. UK Polar Data Centre, Natural Environment Research Council, UK Research & Innovation. Retrieved from <https://doi.org/10.5285/ad7d345a-0650-4f44-b7eb-c48e1999086b'>. Accessed on Oct. 12, 2020.

GERRISH L, FRETWELL P & COOPER P. 2020b. High-resolution vector polygons of Antarctic rock outcrops (7.3) [Data set]. UK Polar Data Centre, Natural Environment Research Council, UK Research & Innovation. Retrieved from <https://doi.org/10.5285/cbacce42-2fdc-4f06-bdc2-73b6c66aa641'>. Accessed on Oct. 12, 2020.

HILLEBRAND FL, BREMER UF, ARIGONY-NETO J, ROSA CN DA, MENDES JR CW, COSTI J, FREITAS MWD DE & SCHARDONG F. 2021. Comparison between atmospheric reanalysis models ERA5 and ERA-Interim at the North Antarctic Peninsula region. Ann Am Assoc Geogr 111: 1147-1159.

HUANG L, LI Z, TIAN BS, CHEN Q & ZHOU JM. 2013. Monitoring glacier zones and snow/firn line changes in the Qinghai-Tibetean plateau using C-band SAR imagery. Remote Sens Environ 137: 17-30.

JEZEK KC, DRINKWATER MR, CRAWFORD JP, BINDSCHADLER R & KWOK R. 1993. Analysis of synthetic aperture radar data collected over southwestern Greenland ice sheet. J Glaciol 131: 119-132.

JEZEK KC, GOGINENI P & SHANABLEH M. 1994. Radar measurements of melt zones on the Greenland ice sheet. Geophys Res Lett 21: 33-36.

JONES ME, BROMWICH DH, NICOLAS JP, CARRASCO J, PLAVCOVÁ E, ZOU X & WANG SH. 2019. Sixty Years of Widespread Warming in the Southern Middle and High Latitudes (1957-2016). J Clim 32: 6875-6898.

LIU H, JEZEK KC & LI B. 1999. Development of Antarctic digital elevation model by integrating cartographic and remotely sensed data. J Geophys Res 104: 23199-23213.

LIU H, JEZEK KC, ZHAO L & ZHAO Z. 2001. Radarsat Antarctic Mapping Project digital elevation model version 2. Boulder, National Snow and Ice Data Center. Retrieved from <http://nsidc.org/data/nsidc-0082.html>. Accessed on Oct. 12, 2020.

LIU H, WANG L & JEZEK KC. 2006. Automated delineation of dry and melt snow zones in Antarctica using active and passive microwave observations from space. IEEE Trans Geosci Remote Sens 44: 2152-2163.

MENDES JR CW, ARIGONY-NETO J, RIBEIRO RR & SIMÕES JC. 2009. Uso de imagens ERS SAR no monitoramento de zonas superficiais de neve e gelo da região nordeste da Península Antártica. Pesqui em Geocienc 36: 203-222.

MORA C, VIEIRA G & RAMOS M. 2013. Evaluation of Envisat ASAR IMP imagery for snow mapping at varying spatial resolution (Deception Island, South Shetlands – Antarctica). In: HAMBREY MJ et al. (Eds), Antarctic Palaeoenvironments and Earth-Surface Processes, London: Geological Society of London 381: 481-493.

MORRIS EM & VAUGHAN DG. 2003. Spatial and temporal variation of surface temperature on the Antarctic Peninsula and the limit of variability of ice shelves. In: DOMACK E et al. (Eds), Antarctic Peninsula climate variability historical and paleoenvironmental perspectives. Washington: American Geophysical Research, p. 61-68.

PARTINGTON KC. 1998. Discrimination of glacier facies using multi-temporal SAR data. J Glaciol 44: 42-53.

PATERSON WSB. 1994. The physics of glaciers. Amsterdam: Elsevier, 480 p.

PEEL D. 1992. Spatial temperature and accumulation rate variations in the Antarctic Peninsula. In Morris EM (Ed), The Contribution of Antarctic Peninsula Ice to Sea Level Rise: Report for the Commission of the European Communities Project EPOC-CT90-0015. Cambridge: British Antarctic Survey, p. 11-15.

RAMAGE JM & ISACKS BL. 2003. Interannual variations of snowmelt and refreeze timing in southeast Alaskan icefields, USA. J Glaciol 49: 102-116.

RAU F. 2003. The upward shift of the dry snow line on the northern Antarctic Peninsula. EARSel e Proceedings 2: 113-121.

RAU F & BRAUN M. 2002. The regional distribution of the dry snow zone on the Antarctic Peninsula north of 70° south. Ann Glaciol 34: 95-100.

RAU F, BRAUN M, FRIEDRICH F, WEBER F & GOBMANN H. 2001. Radar glacier zones and their boundaries as indicators of glacier mass balance and climatic variability. EARSeL e Proceedings 1: 317-327.

RAU F, MAUZ F, DE ANGELIS H, JAÑA R, ARIGONY-NETO J, SKVARCA P, VOGT S, SAURER H & GOßMANN H. 2004. Variations of glacier frontal positions on the northern Antarctic Peninsula. Ann Glaciol 39: 525-530.

REES WG & SATCHELL MJF. 1997. The effect of median filtering on synthetic aperture radar images. Int J Remote Sens 18: 2887-2893.

ROSICH B & MEADOWS P. 2004. Absolute calibration of ASAR Level 1 products generated with PF-ASAR. Technical Note. Document ESA/ESRIN, ENVI-CLVL-EOPG-TN-03-0010. Retrieved from <https://earth.esa.int/web/guest/-/absolute-calibration-of-asar-level-1-products-generated-with-pf-asar-4503>. Accessed on Oct. 12, 2020.

SCAMBOS TA, HULBE C, FAHNESTOCK M & BOHLANDERT J. 2000. The link between climate warming and break-up of ice shelves in the Antarctic Peninsula. J Glaciol 154: 516-530.

SCAR. 2000. Antarctic Digital Database Version 3. Documentation. Retrieved from <https://www.scar.org/library/scar-publications/occasional-publications/5241-add-manual-v3/file/>. Accessed on Oct. 12, 2020.

SKVARCA P & DE ANGELIS H. 2003. Impact assessment of regional climatic warming on glaciers and ice shelves of the northeastern Antarctic Peninsula. In: DOMACK E et al. (Eds), Antarctic Peninsula climate variability historical and paleoenvironmental perspectives. Washington: American Geophysical Research, p. 69-78.

STORVOLD R & MALNES E. 2004. Snow covered area retrieval using ENVISAT ASAR wideswath in mountainous areas. In IGARSS 2004. 2004 IEEE International Geoscience and Remote Sensing Symposium, p. 1845-1848.

TETZNER D, THOMAS E & ALLEN C. 2019. A Validation of ERA5 Reanalysis Data in the Southern Antarctic Peninsula-Ellsworth Land Region, and Its Implications for Ice Core Studies. Geosciences 9: 289-306.

THAKUR PK, GARG PK, AGGARWAL SP, GARG RD & MANI S. 2013. Snow Cover Area Mapping Using Synthetic Aperture

Radar in Manali Watershed of Beas River in the Northwest Himalayas. J Indian Soc Remote Sens 41: 933-945.

TRUSEL LD, FREY KE & DAS SB. 2012. Antarctic surface melting dynamics: Enhanced perspectives from radar scatterometer data. J Geophys Res 117: 1-15.

TRUSEL LD, FREY KE, DAS SB & MUNNEKE PK. 2013. Satellite-based estimates of Antarctic surface meltwater fluxes. Geophys Res Lett 40: 6148-6153.

VAN DEN BROEKE M. 2005. Strong surface melting preceded collapse of Antarctic Peninsula ice shelf. Geophys Res Lett 32: 1-4.

VOGT S & BRAUN M. 2004. Influence of glaciers and snow cover on terrestrial and marine ecosystems as revealed by remotely sensed data. Pesqui Antart Bras 4: 105-118.

ZHOU C & ZHENG L. 2017. Mapping Radar Glacier Zones and Dry Snow Line in the Antarctic Peninsula Using Sentinel-1 Images. Remote Sens 9: 1-11.

ZHOU C, LIU Y & ZHENG L. IN PRESS. Satellite-derived dry-snow line as an indicator of the local climate on the Antarctic Peninsula. J Glaciol 68: 54-64.

How to cite

MENDES JR CW, ARIGONY NETO J, HILLEBRAND FL, DE FREITAS MWD, COSTI J & SIMÕES JC. 2022. Snowmelt retrieval algorithm for the Antarctic Peninsula using SAR imageries. An Acad Bras Cienc 94: e20210217. DOI 10.1590/0001-3765202220210217.

Manuscript received on February 17, 2021;
accepted for publication on October 4, 2021

CLAUDIO W. MENDES JR[1]
https://orcid.org/0000-0003-1745-348X

JORGE ARIGONY NETO[2]
https://orcid.org/0000-0003-4848-2064

FERNANDO L. HILLEBRAND[3]
https://orcid.org/0000-0002-0182-8526

MARCOS W.D. DE FREITAS[4]
https://orcid.org/0000-0001-9879-2584

JULIANA COSTI[2]
https://orcid.org/0000-0001-6220-2343

JEFFERSON C. SIMÕES[4]
https://orcid.org/0000-0001-5555-3401

[1]Universidade Federal do Rio Grande do Sul/UFRGS, Departamento de Geodésia, Av. Bento Gonçalves, 9500, 91509-900 Porto Alegre, RS, Brazil

[2]Universidade Federal do Rio Grande/FURG, Instituto de Oceanografia, Av. Itália, s/n, Km 8, 96201-900 Rio Grande, RS, Brazil

[3]Instituto Federal de Educacão, Ciência e Tecnologia do Rio Grande do Sul/IFRS, Rodovia RS-239, Km 68, Nº 3505, 95700-000 Rolante, RS, Brazil

[4]Universidade Federal do Rio Grande do Sul/UFRGS, Departamento de Geografia, Av. Bento Gonçalves, 9500, 91501-970 Porto Alegre, RS, Brazil

Correspondence to: **Claudio Wilson Mendes Jr**
E-mail: claudio.mendes@ufrgs.br

Author contributions

Claudio Wilson Mendes Jr and Jorge Arigony Neto wrote this manuscript, pre-processed the ASAR images, developed and implemented the classification algorithm, while Fernando Luís Hillebrand and Marcos Wellausen Dias de Freitas performed the WZRZ classification in these images and elaborated figures. Juliana Costi and Jefferson Cardia Simões reviewed and edited this article and made several comments and discussions about its results.